



Friedrich Miescher Institute
for Biomedical Research

Master Thesis

Investigating the stress granule protein G3BP1 with single-molecule imaging of mRNA

Author:

Bastian Th. Eichenberger

Supervisor:

Jeffrey A. Chao and Susan E. Mango

UNIVERSITY OF BASEL
Basel, Switzerland

*A thesis submitted in fulfillment of the requirements for the
degree of Master of Science in Molecular Biology.*

May 2020

Abstract

Stress granules are cytoplasmic, membrane-less organelles containing a plethora of proteins involved in translation initiation and repression and are exclusively formed in stress conditions. This study aimed to better understand the role of stress granules by focussing on a core protein component: Ras GTPase-Activating Protein-Binding Protein 1 (G3BP1). By tethering G3BP1 to specific mRNAs, various single-molecule imaging tools were used to investigate G3BP1's effect on translation (SunTag) and mRNA stability (TREAT). G3BP1 tethering to mRNAs encoding *Renilla* luciferase and SunTag yielded an increase in bulk *Renilla* Luciferase activity but SunTag imaging of translation showed that translation sites had similar intensities, which measures ribosome occupancy, compared to control cells. However, as shown by a TREAT assay to measure 5'-3' mRNA degradation, mRNA stability was significantly increased upon G3BP1 tethering. Lastly, an optimized version of the SunTag translation site imaging tool using a spaghetti-monster-based structural support is presented that can be used in future studies to address many unanswered questions.

Keywords: Stress granules, G3BP1, SunTag Imaging, TREAT, Luciferase assay, mRNA Tethering.

Acknowledgments

First and foremost, I would like to thank Jeff for making this project possible and keeping me (at least somewhat) on the right track and encouraging me to dive deeper into coding. Next, I can count myself lucky for having an awesome supervisor in Daniel who remained critical and always helpful if questions arose. Regarding questions..., I had a few. And without Pratik and Franka many of those would have remained unanswered. They gave me helpful comments on improving this very document and contributed to a pleasant lab atmosphere. In a rather busy time, Varun was friendly enough to clone the smGFP plasmid which made me have more time to focus on other important things at hand. Finally, a big thank you to Susan for accepting being the official part of the university and grading this thesis.

Contents

Abstract	i
Acknowledgments	ii
Contents	iii
1 Introduction	1
1.1 mRNA life cycle	1
1.2 Translation site imaging	4
2 Methods	7
2.1 Key resources	7
2.2 Method details	12
2.3 Quantification and statistical analysis	16
2.4 Data and code availability	18
3 Results	19
3.1 G3BP1 tethering affects mRNA localization	19
3.1.1 Reporter expression is impacted by G3BP1	21
3.1.2 G3BP1 does not alter mRNA translation	22
3.1.3 Transcript stability is affected by G3BP1 tethering	25
3.2 How can the SunTag reporter be improved?	27
4 Discussion	30
Bibliography	32
A Supplementary Methods	42
B Supplementary Figures	46

1

Introduction

1.1 mRNA life cycle

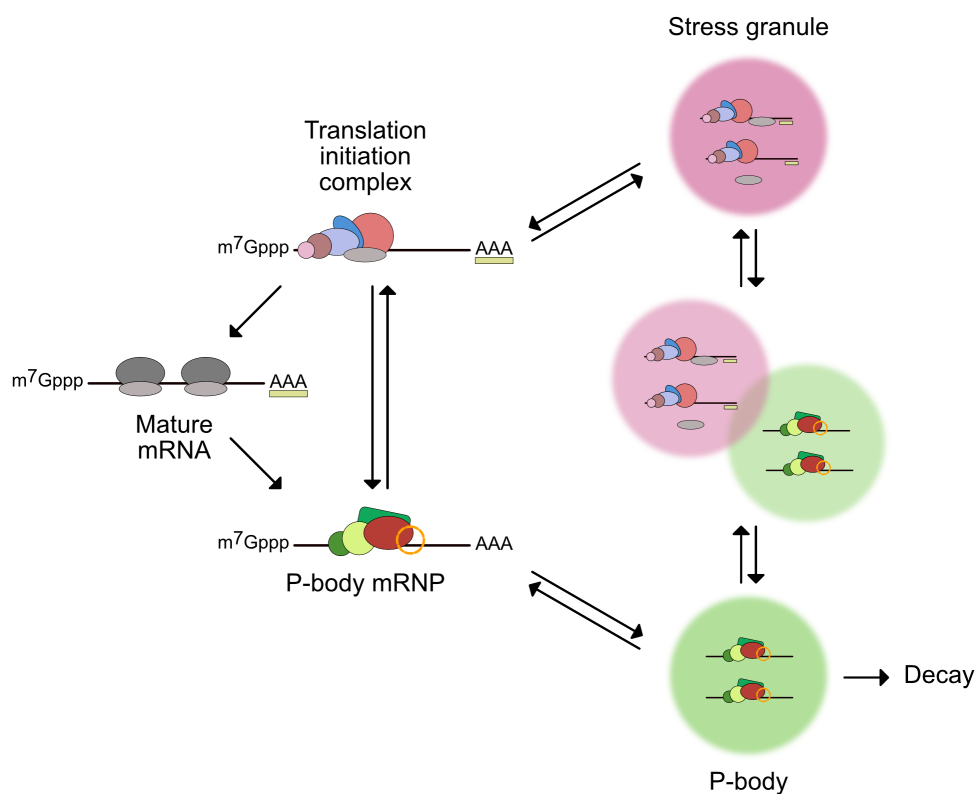
Transcription is the first step in gene expression in which a premature RNA molecule is made from a gene's DNA template. In eukaryotes, splicing, adding a 5' cap and poly-A-tail, as well as binding of cap- and RNA-binding proteins yields mature messenger RNAs (mRNAs). As transcription and translation are compartmentally separated, these mRNAs are then typically exported through nuclear pore complexes, which perforate the nuclear envelope. Once in the cytoplasm, the acquired protein coat determines the fate of the mRNA [1]. One of these fates is translation to produce proteins. This process involves polysome (multiple ribosomes translating an mRNA) assembly and messenger ribonucleoprotein complex remodeling and can occur immediately or delayed, such as in the case of various developmental transcripts (reviewed in [2]). If a protein no longer needs to be produced, polysomes might get disassembled. Based on the interactions of mRNA-binding proteins, mRNAs can now be targeted for degradation (reviewed in [3]). Alternatively, subsets of these mRNAs can be packaged into RNA granules (Figure 1.1A). RNA granules are cytoplasmic, membrane-less, and evolutionarily conserved aggregates containing various proteins involved in translation initiation and repression (reviewed in [4]).

Stress granules (SGs) are a prominent type of RNA granules that exclu-

Chapter 1. Introduction

sively form under stress. Cellular stress arises from various external or internal factors and can trigger the integrated stress response pathway. Typical extrinsic factors range from starvation, infection, hypoxia, the presence of oxidants, and many more. The largest intrinsic factor is endoplasmic reticulum stress through the accumulation of unfolded or misfolded proteins. All of these acti-

A



B

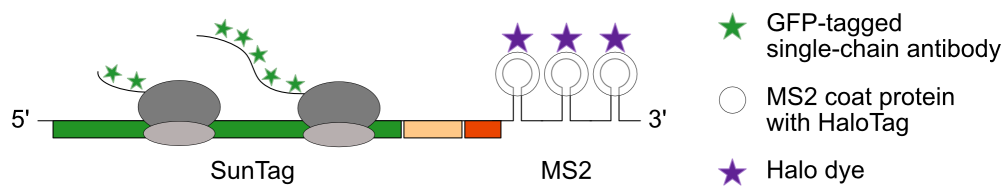


Figure 1.1: (Continued on the following page.)

Chapter 1. Introduction

Figure 1.1: mRNA life cycle and translation site imaging. (A) Overview of a mature, translating mRNAs life cycle. Protein components of the translation initiation complex together with their bound mRNAs can aggregate into membrane-less organelles termed stress granules. A similar type of RNA granule, the P-bodies, have been associated with mRNA decay and a different set of proteins. Both granules can interact and possibly exchange components. (B) Schematic description of SunTag imaging to visualize and quantify translational activity on a single-molecule level. mRNA building blocks (from left to right): SunTag cassette, *Renilla* luciferase, proteotuner tag, and MS2 stem-loops.

vations converge to the phosphorylation of S52 on the α subunit on eukaryotic translation initiation factor 2 (eIF2 α). This phosphorylation deactivates eIF2 α and inhibits global protein synthesis which can lead to an up-regulation of stress-response genes (reviewed in [5]). Multiple immunofluorescence-based studies have shown that SGs showed an enrichment in initiation factors including eIF2 but not for other translation-related machinery components such as the 60S ribosomal subunit [6]. Some proteins found in SGs such as the T-cell intracellular antigen-1 (TIA-1) [7] and Ras GTPase-Activating Protein-Binding Protein 1 (G3BP1) [8] have been found to induce SG formation upon overexpression. The exact nature of SG formation is unknown but various mechanisms from prion-like assembly [9, 10], maturation of mRNA Processing Bodies (P-bodies) (described below) [11], and microtubule involvement have been proposed [12]. While SG formation seems to be a conserved phenomenon throughout eukaryotes, their function also remains unclear. Previous studies have suggested an involvement of SGs in mRNA stability and translational repression (reviewed in [13]). Furthermore, SG assembly coincides with an accumulation of stalled translation preinitiation complexes in conjunction with polysome disassembly and an increase in uncoated cytoplasmic mRNAs [14]. This, along with the observed enrichment of SGs in initiation factors leads to the assumption that SGs exclusively contain translationally repressed mRNAs (reviewed in [15]). However, recent findings from our laboratory have reported

Chapter 1. Introduction

that some SG-localized mRNAs can still be translated [16].

A different type of RNA granules, the P-bodies, were originally described as mouse XRN1p (a highly conserved 5'-3' exonuclease) foci in the cytoplasm [17]. P-bodies, unlike SGs, are present in unstressed physiology. However, stress can further increase their formation (reviewed in [18]). Contrasting SGs, they contain non-overlapping protein components including multiple nucleases that have made them a proposed site of mRNA decay [19].

Many questions regarding RNA granules, and especially SGs, remain largely unanswered. For example, their dynamic formation and disintegration, as well as what determines their composition remains unclear. Several large scale analyses of SGs using spatial proteomics [20, 21, 22] and RNA sequencing [23] approaches have given important insights into the content of SGs but not their function. In a recently published trio of papers [24, 25, 26] a combination of experiments and computational modeling provided more insights into the formation of SGs. They hinted at G3BP1 being a key hub in the SG protein interaction network playing a central role during SG formation by RNA-induced conformational changes. None of these studies, however, gave insights into the biological function that G3BP1 or other SG components exert on single mRNAs. Recently established single-molecule techniques allow for real-time analyses in live cells. Compared with extensively used bulk assays, these give a higher spatio-temporal resolution of cellular processes. In this study, single-molecule imaging techniques will be used to address the effects of the SG-protein G3BP1 on an mRNA's life cycle.

1.2 Translation site imaging

The stellar explosion SUpernova (SunTag) imaging approach allows for live cell imaging-based analysis to visualize and quantify translation sites [27]. The SunTag system relies on three core components: a reporter RNA containing a SunTag cassette and MS2 stem-loops, a green fluorescent protein (GFP)-

Chapter 1. Introduction

tagged single-chain antibody (scFv) against GCN4, and an MS2 coat protein fused to a HaloTag (Figure 1.1B).

The MS2 system has been widely adopted to tag and visualize specific mRNAs. MS2 stem-loops serve as structural motifs and are recognized by the MS2 bacteriophage capsid RNA-binding protein MS2 (MCP) (reviewed in [28]). Typical MS2 tagging involves the visualization of single mRNAs encoding an array of MS2 stem-loops by an MCP-GFP fusion. Multiple MS2 stem-loops are used to increase the local concentration of MCP bound fluorescent molecules allowing for significant signal amplification. Previous studies have used this method to investigate mRNA metabolism by tethering mRNAs to membranes [29], to proteins [30], or to themselves as shown in a recent optogenetic mRNA clustering approach [31].

Currently available standard SunTag cassettes consist of 24 GCN4 epitope repeats that, upon translation and exposure of the GCN4 epitopes, can be recognized and bound by the co-expressed GFP-tagged scFv. As translation continues, more epitopes get synthesized allowing more scFvs to bind. This increases the local concentration and thereby brightens the fluorescent signal. Once translation is terminated, SunTag peptides together with attached scFvs are released from the mRNA causing a decrease in signal intensity. Degradation of the mature protein is increased due to a proteotuner tag that is located C-terminal of the SunTag cassette and that targets the newly formed protein for proteasomal degradation [32]. The MS2 coat protein-HaloTag fusion in conjunction with a soluble Halo dye is used to visualize the MS2 stem loops on the reporter RNA described above. Taken together, the system allows for accurate tracking of single RNAs and simultaneous quantification of translation.

This study focuses on the understanding of how SGs form and how they function. Using modified components of the SunTag imaging system, G3BP1 is used as the main antagonist to provide interesting insights into the unknown world of SGs. G3BP1 will be tethered to a reporter mRNA by fusion to MCP-Halo. Single-molecule imaging tools including SunTag will be used to investi-

Chapter 1. Introduction

gate the effects of an increased local concentration of SG proteins on mRNA dynamics. Lastly, an improvement to the existing SunTag system is proposed.

2

Methods

2.1 Key resources

Table 2.1: Antibodies

Reagent or Resource	Source	Identifier
Alexa Fluor 647	Abcam	ab150075
TIA-1	Abcam	ab40693

Table 2.2: Experimental Models: Cell lines

Reagent or Resource	Source	Identifier
Hela 11ht	Weidenfeld et al., 2009 [33]	N/A
Hela 11ht + scFv-GFP + <i>Renilla-MS2</i>	This study	N/A
Hela 11ht + scFv-GFP + smGCN4- <i>Renilla-MS2</i>	This study	N/A
Hela 11ht + scFv-GFP + SunTag- <i>Renilla-MS2</i>	This study	N/A
Hela 11ht + TREAT	This study	N/A

Chapter 2. Methods

Table 2.3: Chemicals and Peptides

Reagent or Resource	Source	Identifier
Amino-11-ddUTP	Lumiprobe	15040
Atto 647N NHS ester	Sigma-Aldrich	AD 647N-31
Bovine serum albumin	Sigma-Aldrich	A2153-50G
Dextran sulfate	Sigma	D6001-50G
Doxycycline	Sigma	D3891-1G
FluoroBrite DMEM	Life Technologies	A1896703
Formamide (deionized)	Chemicon	S4117
Ganciclovir	Sigma-Aldrich	G2536-100MG
JF585 HaloTag ligand	Grimm et al., 2015, 2017 [34, 35]	N/A
Lipofectamine 2000	Invitrogen	11668019
Opti-MEM™	Gibco	31985070
Paraformaldehyde (aqueous)	20% Electron Microscopy Sciences	15713
ProLong Gold Antifade Mountant	Molecular Probes, Life Technologies	P36935
Puromycin	Invivogen	ant-pr-1
Sodium Arsenite solution	Sigma	35000-1L-R

Table 2.4: Critical Commercial Assays

Reagent or Resource	Source	Identifier
<i>continues on next page</i>		

Chapter 2. Methods

Reagent or Resource	Source	Identifier
Bradford Protein Assay	Biorad	5000006
<i>Renilla</i> Luciferase Assay System	Promega	E2810

Table 2.5: Oligonucleotides

Reagent or Resource	Source	Identifier
Oligodeoxyribonucleotides and primers are listed in Appendix A.	N/A	N/A

Table 2.6: Recombinant DNA

Reagent or Resource	Source	Identifier
G3BP1-GFP-GFP	Wilbertz et al., 2019 [36]	Addgene #119950
NLS-stdMCP-stdHalo	Voigt et al., 2017 [37]	Addgene #104999
NLS-stdMCP-stdHalo-G3BP1	This Study	N/A
NLS-stdMCP-stdHalo-Rh1	This Study	N/A
pCAGGS-FLPe-IRESpuro	Beard et al., 2006 [38]	Addgene #20733
<i>Renilla</i> -MS2v5	This Study	N/A
scFv-GFP	Voigt et al., 2017 [37]	Addgene #104998

continues on next page

Chapter 2. Methods

Reagent or Resource	Source	Identifier
smGCN4- <i>Renilla</i> -MS2v5	This study	N/A
SunTag- <i>Renilla</i> -MS2v5	Wilbertz et al., 2019 [36]	Addgene #119945
SunTag- <i>Renilla</i> -PP7-MS2v4	Horvathova et al., 2017 [39]	N/A

Table 2.7: Critical Equipment

Reagent or Resource	Source	Identifier
405 iBeam Smart	Toptica Photonics	N/A
488 iBeam Smart	Toptica Photonics	N/A
561 Cobolt Jive	Cobolt	N/A
639 iBeam Smart	Toptica Photonics	N/A
96-Well White Polystyrene Microplates	Costar	07-200-589
CFI Plan Apochromat Lambda 100x Oil/1.45 Objective	Nikon	N/A
CSU-W1 Confocal Scanner Unit	Yokogawa	N/A
Glass Coverslips	Paul Marienfeld GmbH	117580
iXon-Ultra-888 EMCCD Cameras	Andor	N/A
Mithras Multimode Microplate Reader LB 940	Berthold	38099

continues on next page

Chapter 2. Methods

Reagent or Resource	Source	Identifier
MS-2000 Motorized Stage	Applied Scientific Instrumentation	N/A
TetraSpeck™ Fluorescent Microspheres Size Kit	Thermo Fisher Scientific	T14792
Ti2-E Eclipse Inverted Microscope	Nikon	N/A
VS-Homogenizer	Visitron Systems GmbH	N/A

Table 2.8: Software and Algorithms

Reagent or Resource	Source	Identifier
Affinity Designer 1.8.2	Serif (Europe) Ltd	affinity.serif.com/designer/
Benchling 2020	Benchling	benchling.com
Fiji 2.0.0-rc-69/1.52p	Schindelin et al., 2012 [40]	fiji.sc
Fluffy 0.2.2	Eichenberger, 2020 [41]	github.com/BBQuercus/fluffy
KNIME 3.7.2	Berthold et al., 2009 [42]	knime.com/knime-analytics-platform
PyMOL 2.3.3	Schrodinger LLC.	pymol.org
Python 3.7.4	Python Software Foundation	python.org
TrackMate v5.2.0	Tinevez et al., 2017 [43]	imagej.net/TrackMate

continues on next page

Chapter 2. Methods

Reagent or Resource	Source	Identifier
VisiView 4.4.0	Visitron Systems GmbH	visitron.de/ products/ visiviewr-software

2.2 Method details

Cell lines and culture details

The previously described HeLa-11ht cell line [33] was used for this study. The integrated Flp-RMCE (recombinase-mediated cassette exchange) site allows for controlled, single-copy, genomic integration of a target gene. In addition, to induce inserted target genes reversibly with doxycycline, cells are expressing a reverse tetracycline controlled transactivator (rtTA2S-M2). Dulbecco's Modified Eagle Medium (DMEM) containing 4.5 g/l glucose, 100 U/ml Penicillin, 100 µg/ml Streptomycin, 4 mM L-Glutamine, and 10% v/v Fetal Bovine Serum (FBS) was used to culture HeLa cells. Cells were maintained at 37°C with 5% CO₂. Transient transfections were performed with Lipofectamine 2000 transfection reagent (Invitrogen) with Opti-MEM reduced serum medium (Gibco) according to manufacturer's instructions but scaled down to 0.5 µg plasmid DNA and 2 µl Lipofectamine 2000 per 1 ml growth medium.

Plasmid construction

To generate the G3BP1 coat protein fusion, the genomic sequence encoding the full-length G3BP1 Isoform 1 (Q13283-1) was inserted in-frame, downstream of the HaloTag sequence. A 33 nt linker sequence was kept between HaloTag and G3BP1 to promote flexibility between the domains. Assembly was performed by PCR amplification of G3BP1 and the MCP-Halo-linker backbone, followed by Gibson cloning [44]. The resulting construct contains a constitutive UbiC promoter, SV40 NLS (nuclear localization signal), stdMCP (MS2 coat protein), HaloTag, 33 nt linker sequence, G3BP1 with a stop codon, and

Chapter 2. Methods

a Woodchuck Hepatitis Virus Posttranscriptional Regulatory Element (WPRE) improving expression in lentiviral transfection (Supplementary Figure B.3).

The smGCN4 reporter sequence containing GCN4 epitopes was synthesized into a pUC57-Kan expression vector. Assembly was performed by PCR amplification of smGCN4 and the *Renilla*-MS2v5 backbone followed by Gibson cloning. The resulting plasmid contains a Tet-CMV (cytomegalovirus) promoter followed by smGCN4, *Renilla* luciferase, FKBP domain with a stop codon, MS2v5 stem-loop cassette (24x), CTE (constitutive transport element, and SV40 polyA tail (Supplementary Figure B.4).

Reporter cell line generation

A day before selection, HeLa cells were seeded into a 6-well plate. The targeting plasmid containing the reporter (2 µg) and pCAGGS-FLPe-IRESpuo plasmid (2 µg) were transfected using Lipofectamine 2000 (Invitrogen) according to manufacturers' protocol [38]. On the next day, cells were preselected with 5 µl/ml puromycin (Invivogen). Two days later, the puromycin-containing medium was removed and replaced with fresh growth medium containing 50 µM ganciclovir (Sigma-Aldrich). The selection was performed for 10-14 days to get resistant colonies that had undergone RCME. Single-cell sorting into a 96-well plate was performed. Clones were tested for reporter expression using luciferase assays.

***Renilla* luciferase assays**

Reporter production was measured with Promega's *Renilla* Luciferase Assay System. The described cell lines were seeded on 12-well plates. The next day, plasmid DNA was transfected once cells reached approximately 70% confluence as described above. On the subsequent day, the expression of reporters was induced with 1 µg/ml doxycycline (Sigma) for 3 hours unless otherwise specified. Stress was induced by adding 1 mM/ml sodium arsenite (Sigma) for the last 1 hour of induction. To measure recovery, cells were washed twice with

Chapter 2. Methods

phosphate-buffered saline (PBS) and replaced with fresh culturing medium. At the specified time points, cells were washed once with PBS and lysed with 250 µl Passive Lysis Buffer per well. To ensure full cellular lysis, plates were gently shaken for 15 minutes at room temperature. 30 µl lysate was transferred to 96-well EIA/RIA Plate (Costar) in triplicates. Bioluminescence was measured 2 seconds after injecting 12 µl *Renilla* Luciferase Assay Reagent per well. Measurements were performed on the Mithras Multimode Microplate Reader LB 940 (Berthold). Data were normalized by protein concentration measured by standard Bradford Protein Assay (Biorad). Means of at least 3 biological replicates (each with 3 described technical replicates) were calculated.

Single-molecule fluorescence in situ hybridization (FISH)

Single-molecule RNA detection against the *Renilla* luciferase coding sequence and MS2 (v5) was performed using Stellaris FISH probes (Biosearch Technologies). Probes targeting MS2 (v4) were made by enzymatic oligonucleotide labeling [45] with Amino-11-ddUTP (Lumiprobe) and Atto647-NHS (ATTO-TEC).

Cells were seeded on glass coverslips (Paul Marienfeld GmbH) placed in 12-well plates. The next day, cells were transfected as indicated. On the subsequent day, cells were treated as indicated, followed by two washes with PBS and fixation in 4% paraformaldehyde (Electron Microscopy Sciences) diluted in PBS for 5 minutes. Cells were washed thrice with PBS and permeabilized with 0.5% Triton X-100 diluted in PBS for 5 minutes (if immunofluorescence was performed) or overnight at 4°C in 70% ethanol. Cells were washed two more times with PBS and prehybridized with wash buffer (2x SSC (Invitrogen), 10% v/v formamide (Abcam)) twice for 5 minutes. Coverslips were then incubated between 4 and 16 hours with hybridization solution (2x SSC, 10% v/v formamide, 10% v/v dextran sulfate, 0.5% v/v bovine serum albumin (BSA), 200 nM FISH probes) at 37°C in humidified chambers. Cells were washed once more with wash buffer for 30 minutes and twice with PBS. Immunofluorescence staining was performed according to the "Immunofluorescence" sec-

Chapter 2. Methods

tion from BSA blocking to mounting. Samples were then mounted on ProLong Gold Antifade Mountant with DAPI. Imaging was performed as described in the “Live-cell imaging” section using sequential, single-camera acquisition.

Immunofluorescence

Cells were seeded on glass coverslips (Paul Marienfeld GmbH) placed in 12-well plates. The next day, cells were transfected as indicated. On the subsequent day, cells were treated as indicated, followed by two washes with PBS and fixation in 4% v/v paraformaldehyde (Electron Microscopy Sciences) diluted in PBS for 5 minutes. Cells were washed thrice with PBS and permeabilized with 0.5% v/v Triton X-100 diluted in PBS for 5 minutes. Cells were washed two more times in PBS and incubated in 3% w/v BSA (Sigma-Aldrich) diluted in PBS for 1 hour. Primary antibodies (diluted in 1% w/v BSA in PBS) were incubated for 1 hour at room temperature or overnight at 4°C. After washing three times with PBS, the cells were incubated with secondary antibodies (diluted in 1% w/v BSA in PBS) for 1 hour at room temperature. Cells were washed twice with PBS and mounted on glass slides in ProLong Gold Antifade Mountant with DAPI. Imaging was performed as described in the “Live-cell imaging” section using sequential, single-camera acquisition.

Live-cell imaging

Cells were seeded on 35 mm glass-bottom μ -Dish (ibidi GmbH). The next day, cells were transfected as indicated. On the subsequent day, cells were treated as indicated. During the last 15 minutes of treatment, the medium was supplemented with JF585 HaloTag ligand, obtained from L. Lavis (Janelia Research Campus) [34, 35], at 100 nM final concentration. After incubation, cells were washed once with PBS and kept in FluoroBrite DMEM (Life Technologies) containing 10% v/v FBS and 4 mM L-glutamine. Cells were imaged within 15 minutes of medium exchange on an inverted Ti2-E Eclipse microscope (Nikon) with a CSU-W1 Confocal Scanner Unit (Yokogawa), two back-illuminated EM-

Chapter 2. Methods

CCD cameras iXon-Ultra-888 (Andor), an MS-2000 motorized stage (Applied Scientific Instrumentation), and VisiView imaging software (Visitron Systems GmbH). Specimens were illuminated with 561 Cobolt Jive (Cobolt), 405 iBeam Smart, 488 iBeam Smart, and 639 iBeam Smart lasers (Toptica Photonics) and a VS-Homogenizer (Visitron Systems GmbH). All images were acquired with a CFI Plan Apochromat Lambda 100X Oil/1.45 objective (Nikon). This setup results in a pixel size of 130 nm. Unless otherwise indicated, excitation was performed with a 50 ms exposure time in a single plane. The second camera was used to detect the 488 nm channel. To ensure proper camera alignment, TetraSpeck™ Fluorescent Microspheres Size Kit (Thermo Fisher Scientific) was used to image 0.5 μ m fluorescent beads after each imaging session. Cells were maintained at 37°C and 5% CO₂ within an incubation box.

2.3 Quantification and statistical analysis

Detection of mRNA spots from smFISH and colocalization

Using custom-built python scripts, images were registered and maximum intensity projected in all channels. Cells were segmented in two steps. First, a sequential workflow comprising Gaussian filtering steps, Otsu thresholding [46], and distance transform calculations of the DAPI channel (405 nm) was used to segment individual nuclei. Subsequently, the nuclei were used as seeds to perform a watershed segmentation into a previously thresholded cytoplasmic map. Cytoplasmic channels were chosen based on their signal uniformity (561 nm *Renilla* luciferase or MS2v5 probe channel). SGs were segmented in Fluffy [41]. mRNA spots were detected with a Laplacian of Gaussian filter. Thresholds for cellular segmentation and spot detection were kept constant throughout a dataset. To colocalize mRNA spots, Euclidean distances were calculated between spots across both channels. To ensure proper channel-to-channel association of mRNA spots, cells with a high spot

Chapter 2. Methods

density were filtered out. Two mRNAs were considered as colocalized when their coordinates are less than 2 px (240 nm) apart.

Processing of live-cell imaging data

Images of the fluorescent beads were used to perform channel alignment. Using the pystackreg python package [47] an affine transformation was registered. This model was subsequently re-applied to all images acquired with the secondary camera. Fiji [40] was used to create representative images via cropping, brightness adjustments, channel merging, and scale bar annotation. TrackMate [43] was used to display tracked particles.

Quantification of translational status

Tracking-based quantification of translation was performed using a KNIME [42] workflow described in Mateju et al. [16] in section “Track-based analysis of translational status and colocalization” without including the described SG association component.

Statistics

Results are presented as the mean \pm confidence interval (95%) of independent experiments. Significant differences between variables are based on independent sample t-tests. P-values are indicated using stars in each figure. Each star corresponds to the following p-values:

- ns: $5e^{-2} < p \leq 1$
- *: $e^{-2} < p \leq 5e^{-2}$
- **: $e^{-3} < p \leq e^{-2}$
- ***: $e^{-4} < p \leq e^{-3}$
- ****: $p \leq e^{-4}$

2.4 Data and code availability

The code used to analyze and visualize the data together with plasmid maps is available on GitHub¹. All data supporting the findings of this study are available on request.

¹ <https://github.com/BBQuercus/master-thesis>

3

Results

3.1 G3BP1 tethering affects mRNA localization

Proteins of the G3BP RNA-binding family are key components of SGs. In mammals, G3BP1 (and its paralog G3BP2) were reported to be essential in nucleating the formation of SGs [48]. SGs can not only be induced by stress (e.g. sodium arsenite) but also by the overexpression of G3BPs [8]. In addition, a recent proteomics-based study by Markmiller et al. [20] showed that "many well-characterized SG proteins (e.g., G3BP1, TIA1, CAPRIN1, PABPC1, FMR1, and ATXN2) were identified as highly significant interactors" suggesting an interplay of SG proteins even in unstressed conditions. This finding might suggest the formation of an mRNP complex containing SG proteins allowing for a rapid assembly of SGs.

The exact role of G3BPs in SG assembly as well as in unstressed cells is still largely unknown. As reviewed in Alam and Kennedy [49] various functions have been attributed to this protein family. These range from transcript destabilization and repression to the polar opposite in transcript stabilization. Furthermore, G3BPs also showed effects on transcript localization and sequestration to virus-induced foci (reviewed in [50]). The only consensus is G3BP's involvement in mRNA translational control. The subsequent experiments attempt to clarify this disunity by analyzing G3BP1's effect on mRNA transcripts at a single-molecule level. For this reason, I designed an assay to directly tether G3BP1 to reporter mRNAs and thereby allow its effect on trans-

Chapter 3. Results

lation and mRNA degradation to be measured as well as to promote mRNA accumulation into SGs.

This study focussed on a reporter RNA containing a SunTag cassette, the gene encoding for *Renilla* luciferase, a proteotuner tag, and MS2 stem-loops (Figure 3.1A). In order to promote mRNA recruitment to SGs, I fused G3BP1 MCP-Halo (abbreviated as MCPG3). The construct was validated by FISH against the reporter RNA followed by immunofluorescence for the endogenous

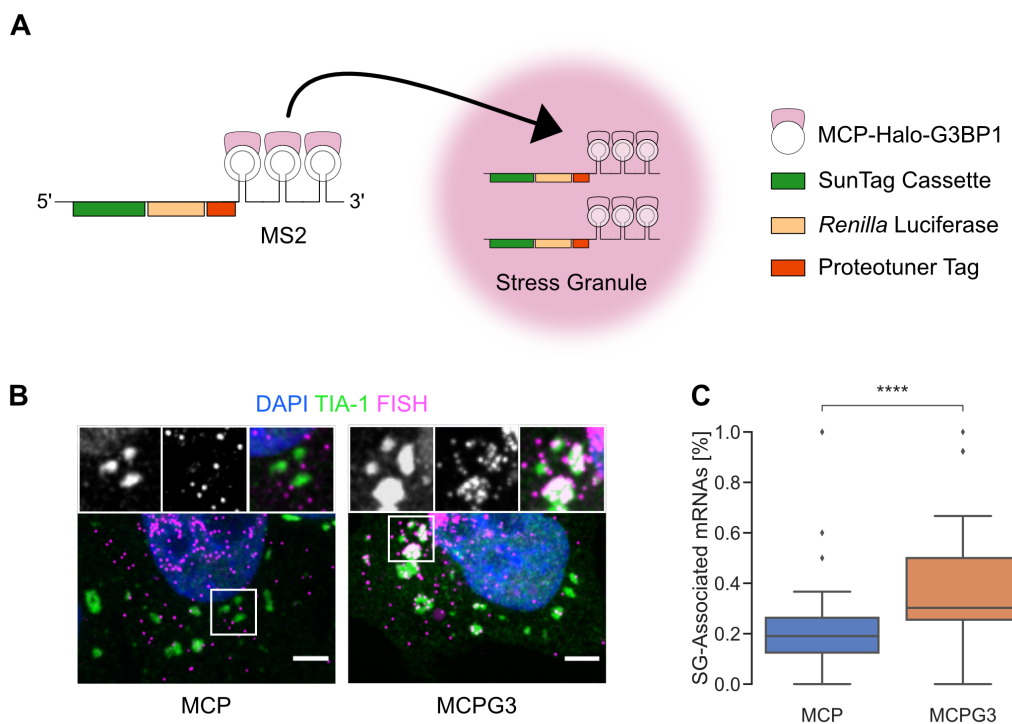


Figure 3.1: Design of MCPG3. (A) Schematic depiction of MCPG3 function. (B) Representative fluorescence images of the SG marker TIA-1 and the tethered RNAs. To induce SGs, cells were treated with sodium arsenite (1 mM) for 1 hour. Panels show TIA-1, FISH, Merge respectively. Scale bars, 10 μ m. (C) Quantification of the mRNA recruitment to SGs. Number of cells quantified (left to right): 27, 21. Two replicates.

Chapter 3. Results

SG marker TIA-1 [7] (Figure 3.1B). SGs were induced by sodium arsenite treatment (1 mM for 1 hour). As a control, an identical construct only lacking G3BP1 fusion was used. The G3BP1 fusion construct resulted in a significant difference in SG association (Figure 3.1C). MCPG3 shows an approximately two-fold increase in SG associated mRNAs compared to the control while not causing mRNA aggregation in unstressed conditions (Supplementary Figure B.1). In addition, both the area and intensity of SGs seem to not be affected by the G3BP1 fusion (Supplementary Figures B.2A and B.2B respectively). Taken together, fusing G3BP1 to MCP seems to be a reliable way to recruit functional G3BP1 to the local vicinity of mRNAs and thereby promote localization to SGs.

3.1.1 Reporter expression is impacted by G3BP1

Having shown that G3BP1 can be recruited to mRNAs, I wanted to investigate the effect on translational activity. *Renilla* luciferase assays are used to measure reporter expression on a global level. As G3BP1 was shown to be involved in stress-induced events as well as in unstressed conditions, the luciferase activity at multiple time points in unstressed cells as well as in cells recovering from oxidative stress was measured.

In unstressed cells, G3BP1 recruitment resulted in increased luciferase readings over time (Figure 3.2A). This suggests that the presence of G3BP1 on a transcript might promote protein synthesis. Comparing both constructs during stress recovery, one can observe a slightly less significant but still noticeable increase in luciferase activity for MCPG3 expressing cells (Figure 3.2B). During stress conditions, most mRNAs get translationally silenced [36] which explains the comparative dropoff in luciferase activity directly after stress. Interestingly, the largest effects are at later time points and during non-stress conditions while not being immediately after stress recovery. Preliminary experiments using different durations of stress have yielded similar results. SGs have been observed to persist between a few minutes to hours after removal

Chapter 3. Results

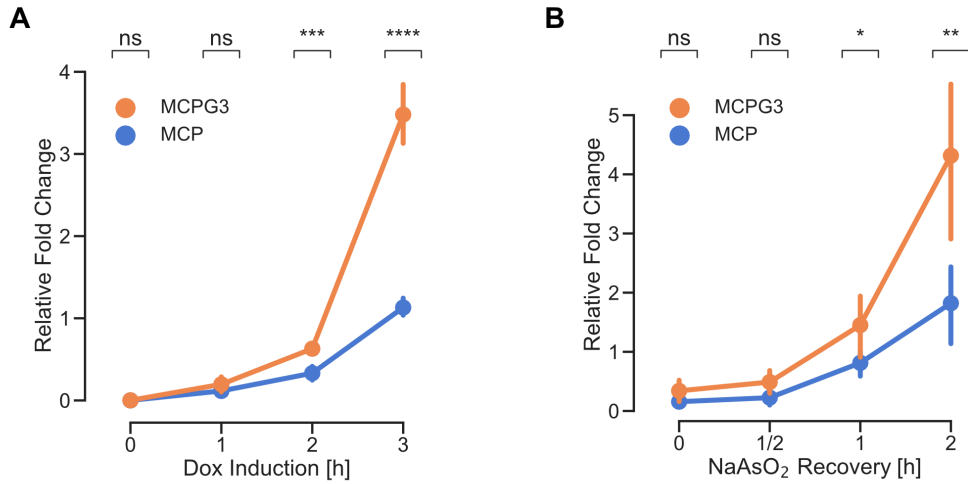


Figure 3.2: G3BP1 tethering increases reporter translational activity. (A) Luciferase assays at different time points during induction. (B) Sodium arsenite stress recovery time points after induction. Cells were induced for 3 hours and stressed with sodium arsenite (1 mM) in the last hour. Timepoint capture started immediately after washing out the stressor. (A and B) Data normalized to the 3-hour induction condition of MCP. Five replicates.

of the stressor [51, 36]. This correlates with the time when an increase in luciferase activity can be observed again.

3.1.2 G3BP1 does not alter mRNA translation

The observed differences in luciferase activity described in Section 3.1.1 can result from various causes. These differences in reporter protein synthesis levels could arise from an increase in translational activity of mRNAs or an increase in mRNA stability. To investigate the former possibility, I decided to use SunTag imaging, to directly quantify translational activity (see Section 1.2).

In SunTag imaging, the fluorescence intensity is a direct measure of translation rate. Therefore, to analyze the translation activity of MCPG3-bound mRNAs, the intensity of translation site spots was quantified over at least four

Chapter 3. Results

consecutive timeframes with a maximum of one gap frame.

When comparing SunTag tracks of single mRNAs in unstressed cells expressing MCPG3 or control MCP (Figure 3.3A), both conditions show similar fluorescence intensities suggesting G3BP1 does not have a major effect on mRNA translation rates. Similarly, the grouping of all SunTag tracks measured within a single cell shows comparable mean intensities in cells expressing MCPG3 or control MCP. Equivalently to the image-level analysis, the mean cellular intensities (Figure 3.3B) do not yield different results. The average intensity of all tracks per cell does not appear to be affected by G3BP1 fusion.

As previously mentioned, most mRNAs get translationally silenced during stress conditions [36]. To image translation sites despite this silencing and to investigate if increased recruitment of mRNA to SGs by MCPG3 has an effect on translation rates, images were acquired 15 to 30 minutes after removing the stressor. Nonetheless, cells did not fully recover the translational silencing leading to lower readings of fluorescent intensity in the stress condition compared to unstressed cells. However, in this case, as well, G3BP1 tethering does not lead to significant differences in translational activity.

Lastly, translation can also increase due to a higher number of translating transcripts per cell. However, as is evident from Figure 3.3C the number of translating tracks stays consistent in all experiments. This suggests that G3BP1 does not have a profound impact on translation activity.

Chapter 3. Results

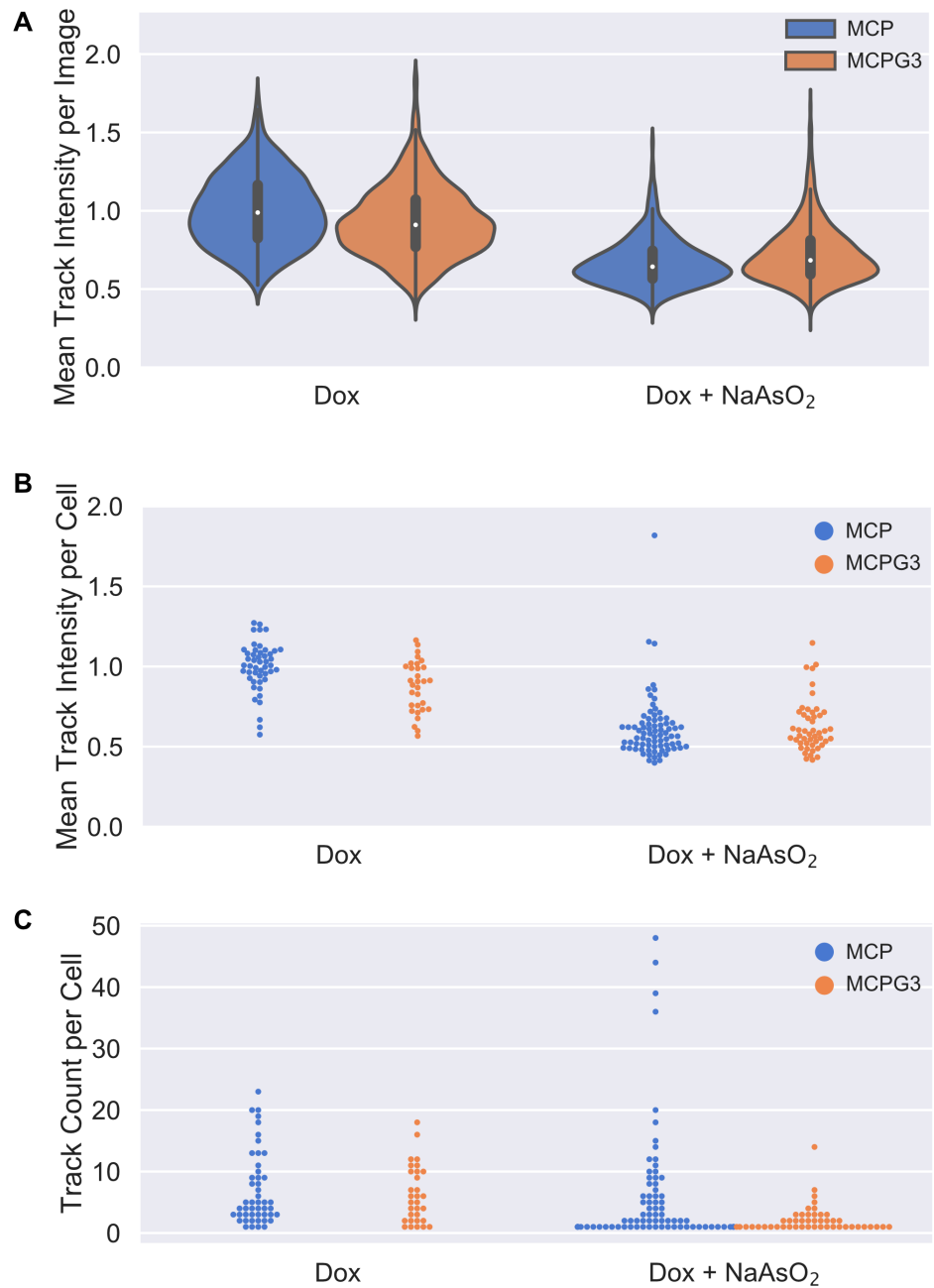


Figure 3.3: (Continued on the following page.)

Chapter 3. Results

Figure 3.3: G3BP1 does not affect translational activity. (A) Distribution of the mean fluorescence intensity of tracked mRNAs in the full-sized image. The total number of tracks (left to right): 715, 1064, 997, 3442. (B) Track intensity averaged per cell. (A and B) Data normalized to the Dox induction condition for MCP. (C) The number of tracks registered per cell. (B and C) The total number of cells (left to right): 48, 77, 31, 48. Single replicate.

3.1.3 Transcript stability is affected by G3BP1 tethering

SunTag measurements (see Section 3.1.2) did not suggest any effect of G3BP1 on translational activity. Alternatively, a decrease in mRNA degradation could also explain the increased *Renilla* luciferase readings. To ask whether G3BP1 has an mRNA stabilizing effect, I compared the half-lives of transcripts between MCPG3 and the control using 3(three)'-RNA end accumulation during turnover (TREAT) [39].

TREAT uses a slightly modified reporter mRNA containing viral RNA pseudo-knot (PK) structures upstream of the MS2 stem-loops. These PKs can block Xrn1 mediated 5'-3' degradation of a transcript by sequestering the 5' phosphate group [52]. Subsequently, by using FISH probes against *Renilla* luciferase upstream of PKs (showing intact mRNAs) and FISH probes against MS2 stem-loops downstream of PKs (showing both intact and degraded mRNAs) one can quantify the number of degradation intermediates.

To look at transcript stabilization, a cell line expressing the aforementioned TREAT mRNA reporter was used. Five time points were chosen to match TREAT half-life after a 1 hour induction followed by thorough washing to remove doxycycline to halt any further transcription. As can be seen in Figure 3.4A, transcripts are exported from the nucleus into the cytosol over the course of the experiment. This suggests that no new transcripts are produced in the nucleus and that MCPG3 does not negatively affect nuclear export.

When comparing the percentage of intact mRNAs, i.e. transcripts still containing FISH spots against both *Renilla* luciferase and MS2, between MCPG3

Chapter 3. Results

and the control, I observed a significant difference (Figure 3.4B). The G3BP1 fusion shows a significant reduction in degraded transcripts compared to the control suggesting an increase in mRNA stability. This effect is not reflected in the translation site-based mRNA count from the SunTag measurements (see Section 3.1.2) which might arise from the nature of the SunTag cassette that will be discussed in the following Section 3.2.

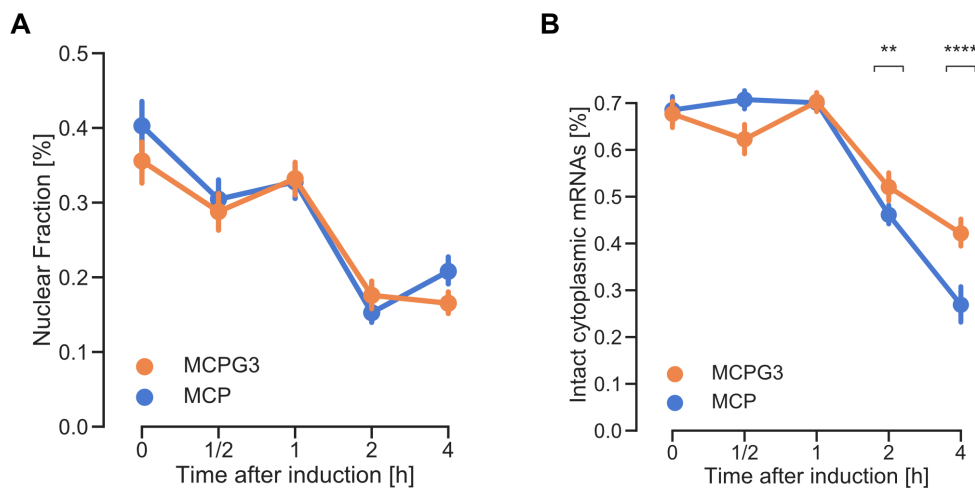


Figure 3.4: mRNA stability increases by G3BP1 tethering. (A) The fraction of nuclear mRNAs (of total cellular mRNAs) at different time points after induction. (B) Percentage of intact cytoplasmic mRNAs at different time points. (A and B) Number of cells quantified (ascending, MCP then MCPG3): 117, 154, 200, 175, 55, 114, 148, 167, 111, 132. Single replicate.

3.2 How can the SunTag reporter be improved?

The original design of the SunTag cassette consists of 24 GCN4 repeats. These completely disordered repeats have previously led to the observations of decreased *Renilla* luciferase activity and lower induction rates than *Renilla* luciferase without SunTag. In an attempt to improve the SunTag based translation imaging system, a spaghetti monster reporter was made. Spaghetti monster green fluorescent proteins (smGFP) are essentially a non-fluorescent green fluorescent protein's (GFP) beta-barrel used to attach small epitope tags [53]. Here, three GCN4 repeats each were placed at the N-terminus, C-terminus, and 10/11-loop of the GFP beta-barrel as shown in Figure 3.5A. Previously, other tags, such as influenza hemagglutinin (HA), were used and visualized with frankenbodies (single-chain antibodies targeting various tags) [54]. In this study, I combined SunTag imaging with smGFP constructs.

Initially, while testing the reporter functionality the new reporter showed an approximative 4-fold increase in luciferase activity compared to the standard SunTag reporter (Figure 3.5B). A *Renilla* reporter was used as control which does not contain any GCN4 repeats. While the smGFP reporter drastically increases activity, it does not yet reach the levels of the control. It must be noted that the control also construct does not contain a proteotuner tag which has lowered the luciferase activity in previous experiments by enhancing the degradation of the tagged protein [55].

To test whether this new reporter allows the visualization of translation sites in live cells, stable cell lines were created and observed after 1 hour of induction. From a representative image in Figure 3.5C, one can see that cells typically have more, slightly dimmer translation sites. Quantification of images showed a significant increase in the number of translation sites per cell compared to the cells expressing the standard SunTag reporter (Figure 3.5D). The brightness of individual spots decreased around 2.7 fold (Figure 3.5E). This decrease can be explained by a lower number of GCN4 repeats available for the scFv to bind. Whereas the standard SunTag has 24 GCN4 repeats,

Chapter 3. Results

smGFP only has 9 leading to a binding site difference of $2.6\bar{6}$ to 1. This suggests that the scFv binds to both tags with full occupancy.

Taken together, this study proposes a new SunTag reporter which improves some of the drawbacks of fusing a largely disordered polypeptide to a protein of interest. This new reporter allows for shorter induction times with higher mRNA numbers.

Chapter 3. Results

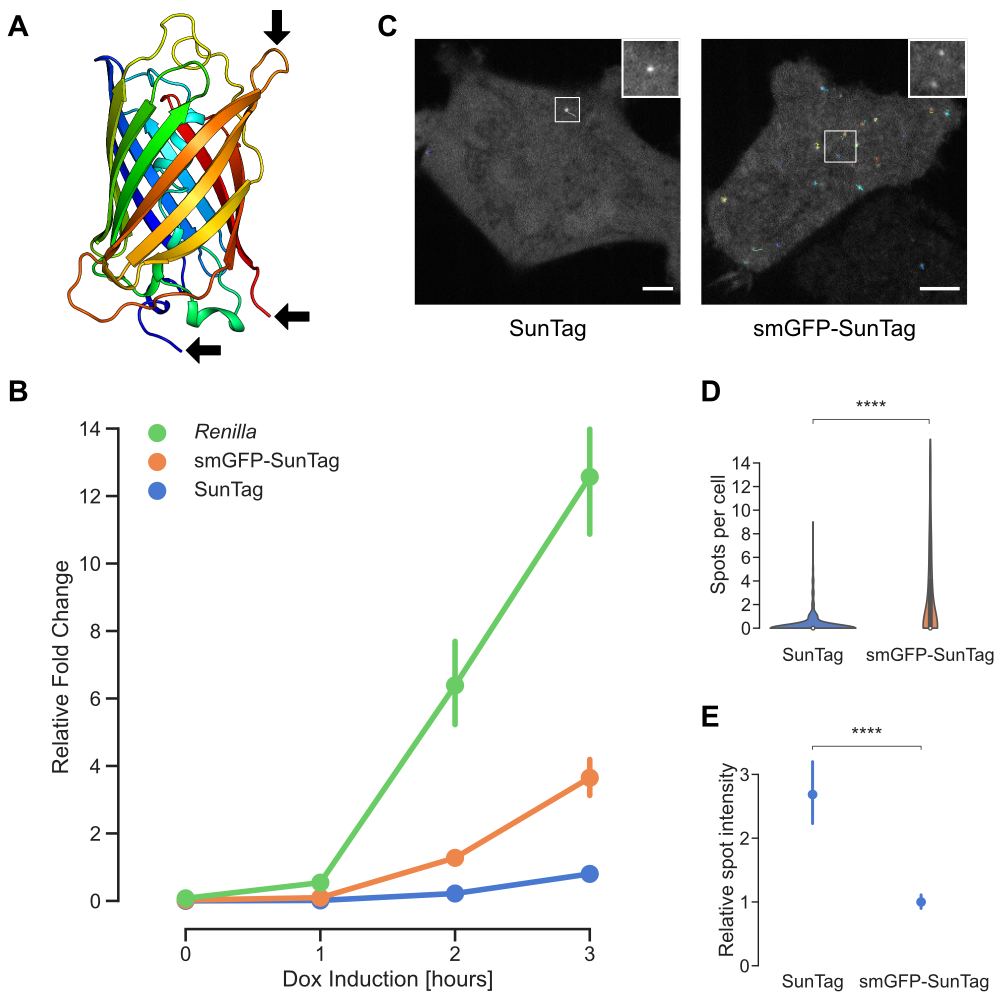


Figure 3.5: smGFP SunTag reporter increases transcript numbers. (A) Structural overview of GCN4 repeat placement on the smGFP beta-barrel (PDB ID: 1GFL [56]). (B) Relative luciferase activity comparing the standard SunTag reporter, the smGFP SunTag reporter (smGFP-SunTag), and a *Renilla* reporter without SunTag cassette. (C) Representative fluorescence images. Each recorded mRNA track is visualized with a unique color. Scale bar, 10 μ m. The inset shows spots from raw images without brightness corrections. (D) Quantification of translation site count per cell. The number of cells quantified (left to right): 286, 233. (E) Average spot intensity normalized to the smGFP reporter. The number of spots quantified (left to right): 36, 39. Two replicates. (C, D, and E) Live imaging experiment with stable cell lines imaged after 1 hour of induction.

4

Discussion

The role of many SG-proteins in unstressed cells is still unclear. An understanding of these proteins, such as G3BP1 could provide important insights into how SGs form and what functional purpose they serve. This study approaches this mystery experimentally.

My results show that fusing G3BP1 to MCP has profound effects on their associated reporter transcripts. First, mRNAs are around two-fold more likely to get recruited to SGs. The nature of transient transfections used for these sets of experiments typically does not achieve complete cellular coverage. Therefore, this likely lowers the measured numbers compared to if all cells were expressing the constructs. Furthermore, due to highly clustered mRNAs in SGs, accurate quantification was proven to be rather difficult, also decreasing the number. Second, G3BP1 has a significant effect on protein expression irrespective of cellular stress. This interesting finding showed that the role of G3BP1 in SGs might just be secondary while its more important function occurs in normal cell homeostasis. As previously proposed, SGs might arise from the necessity to sequester proteins like G3BP1 from mRNA targets in the cytosol [57]. SunTag imaging experiments were performed to observe differences in translational activity. These, however, did not show major differences suggesting that G3BP1 might only have minor roles in translational activity. Interestingly, TREAT assays looking at mRNA stability showed significant differences. This suggests that G3BP1 tethering reduces 5'-3' mRNA degradation. While some recent publications have provided evidence for a decay promoting role of G3BP1 [57, 58], others including this study have sug-

Chapter 4. Discussion

gested the opposite [59, 60, 61]. It must be noted that this mRNA stabilizing effect, while significant, still does not entirely prevent mRNAs from degradation. The molecular mechanisms behind this finding remain unknown but could arise from a microscopic SG-like environment forming around single mRNAs. Even though G3BP1 tethering does not form visible SGs in unstressed cells, the recruitment of SG proteins by G3BP1 could still be sufficient to reduce mRNA degradation. Similarly, G3BP1 could also actively be preventing the recruitment of decay enzymes to their tethered target mRNAs. To follow up on these proposals, it would be necessary to investigate whether the local protein composition changes proximally to tethered mRNAs. A similar experimental setup could also be used to test the mRNA stabilizing effect of other SG-proteins like TIA-1, single G3BP1 domains, or domains enriched in the SG transcriptome such as DEAD-box helicases. Lastly, the direct involvement of G3BP1 on mRNA stabilization during stress conditions has not been investigated and must be addressed to understand the overall role of G3BP1 in mRNA metabolism.

In an effort to increase the expression levels of the currently used SunTag reporter cassette, a novel cassette relying on structural support by smGFP was created. The preliminary results shown here suggest that single-chain antibody occupancies are comparable with the previous version while greatly increasing transcript numbers. This seems to mainly be achieved through more translating transcripts per cell. However, it is still unclear what the underlying cause of the poor induction of the SunTag reporter is. The lower signal intensity has shown to make a track based analysis slightly harder. To counteract this, one could, however, use two or more cassettes, or add more GCN4 repeats at other locations within the structural scaffold. Looking forward, it would be interesting to see if mRNA stability is also affected and how the system can be evolved. Recent progress in single-chain antibodies leads the way to a highly interchangeable system with different tags and fluorescent colors.

Bibliography

- [1] Melissa J. Moore. From birth to death: the complex lives of eukaryotic mRNAs. *Science (New York, N.Y.)*, 309(5740):1514–1518, September 2005.
- [2] Ian A. Swinburne and Pamela A. Silver. Intron Delays and Transcriptional Timing during Development. *Developmental cell*, 14(3):324–330, March 2008.
- [3] Daniel R. Schoenberg and Lynne E. Maquat. Regulation of cytoplasmic mRNA decay. *Nature Reviews Genetics*, 13(4):246–259, April 2012. Number: 4 Publisher: Nature Publishing Group.
- [4] Paul Anderson and Nancy Kedersha. RNA granules. *The Journal of Cell Biology*, 172(6):803–808, March 2006.
- [5] Karolina Pakos-Zebrucka, Izabela Koryga, Katarzyna Mnich, Mila Ljujic, Afshin Samali, and Adrienne M. Gorman. The integrated stress response. *EMBO reports*, 17(10):1374–1395, October 2016.
- [6] Scot R. Kimball, Rick L. Horetsky, David Ron, Leonard S. Jefferson, and Heather P. Harding. Mammalian stress granules represent sites of accumulation of stalled translation initiation complexes. *American Journal of Physiology. Cell Physiology*, 284(2):C273–284, February 2003.
- [7] Nancy L. Kedersha, Mita Gupta, Wei Li, Ira Miller, and Paul Anderson. RNA-Binding Proteins Tia-1 and Tiar Link the Phosphorylation of Eif-2 α to the Assembly of Mammalian Stress Granules. *The Journal of Cell Biology*, 147(7):1431–1442, December 1999.
- [8] Helene Tourrière, Karim Chebli, Latifa Zekri, Brice Courselaud, Jean Marie Blanchard, Edouard Bertrand, and Jamal Tazi. The RasGAP-

Bibliography

- associated endoribonuclease G3BP assembles stress granules. *The Journal of Cell Biology*, 160(6):823–831, March 2003.
- [9] Natalie Gilks, Nancy Kedersha, Maranatha Ayodele, Lily Shen, Georg Stoecklin, Laura M. Dember, and Paul Anderson. Stress granule assembly is mediated by prion-like aggregation of TIA-1. *Molecular Biology of the Cell*, 15(12):5383–5398, December 2004.
- [10] Jenifer E. Shattuck, Kacy R. Paul, Sean M. Cascarina, and Eric D. Ross. The prion-like protein kinase Sky1 is required for efficient stress granule disassembly. *Nature Communications*, 10(1):1–11, August 2019. Number: 1 Publisher: Nature Publishing Group.
- [11] J. Ross Buchan, Denise Muhlrad, and Roy Parker. P bodies promote stress granule assembly in *Saccharomyces cerevisiae*. *The Journal of Cell Biology*, 183(3):441–455, November 2008.
- [12] Pavel A Ivanov, Elena M Chudinova, and Elena S Nadezhina. Disruption of microtubules inhibits cytoplasmic ribonucleoprotein stress granule formation. *Experimental Cell Research*, 290(2):227–233, November 2003.
- [13] J. Ross Buchan and Roy Parker. Eukaryotic Stress Granules: The Ins and Outs of Translation. *Molecular Cell*, 36(6):932–941, December 2009.
- [14] Marc D. Panas, Pavel Ivanov, and Paul Anderson. Mechanistic insights into mammalian stress granule dynamics. *The Journal of Cell Biology*, 215(3):313–323, November 2016.
- [15] María Gabriela Thomas, Mariela Loschi, María Andrea Desbats, and Graciela Lidia Boccaccio. RNA granules: the good, the bad and the ugly. *Cellular signalling*, 23(2):324–334, February 2011.
- [16] Daniel Mateju, Bastian Eichenberger, Jan Eglinger, Gregory Roth, and Jeffrey Chao. Single-molecule imaging reveals translation of mRNAs lo-

Bibliography

- calized to stress granules. *bioRxiv*, page 2020.03.31.018093, April 2020. Publisher: Cold Spring Harbor Laboratory Section: New Results.
- [17] Vladimir I. Bashkirov, Harry Scherthan, Jachen A. Solinger, Jean-Marie Buerstedde, and Wolf-Dietrich Heyer. A Mouse Cytoplasmic Exoribonuclease (mXRN1p) with Preference for G4 Tetraplex Substrates. *Journal of Cell Biology*, 136(4):761–773, February 1997. Publisher: The Rockefeller University Press.
 - [18] Roy Parker and Ujwal Sheth. P bodies and the control of mRNA translation and degradation. *Molecular Cell*, 25(5):635–646, March 2007.
 - [19] Ujwal Sheth and Roy Parker. Decapping and Decay of Messenger RNA Occur in Cytoplasmic Processing Bodies. *Science (New York, N.Y.)*, 300(5620):805–808, May 2003.
 - [20] Sebastian Markmiller, Sahar Soltanieh, Kari L. Server, Raymond Mak, Wenhao Jin, Mark Y. Fang, En-Ching Luo, Florian Krach, Dejun Yang, Anindya Sen, Amit Fulzele, Jacob M. Wozniak, David J. Gonzalez, Mark W. Kankel, Fen-Biao Gao, Eric J. Bennett, Eric Lécuyer, and Gene W. Yeo. Context-Dependent and Disease-Specific Diversity in Protein Interactions within Stress Granules. *Cell*, 172(3):590–604.e13, January 2018.
 - [21] Saumya Jain, Joshua R. Wheeler, Robert W. Walters, Anurag Agrawal, Anthony Barsic, and Roy Parker. ATPase-Modulated Stress Granules Contain a Diverse Proteome and Substructure. *Cell*, 164(3):487–498, January 2016.
 - [22] Ji-Young Youn, Wade H. Dunham, Seo Jung Hong, James D. R. Knight, Mikhail Bashkurov, Ginny I. Chen, Halil Bagci, Bhavisha Rathod, Graham MacLeod, Simon W. M. Eng, Stéphane Angers, Quaid Morris, Marc Fabian, Jean-François Côté, and Anne-Claude Gingras. High-Density

Bibliography

- Proximity Mapping Reveals the Subcellular Organization of mRNA-Associated Granules and Bodies. *Molecular Cell*, 69(3):517–532.e11, February 2018.
- [23] Anthony Khong, Saumya Jain, Tyler Matheny, Joshua R. Wheeler, and Roy Parker. Isolation of mammalian stress granule cores for RNA-Seq analysis. *Methods*, 137:49–54, March 2018.
- [24] Jordina Guillén-Boixet, Andrii Kopach, Alex S. Holehouse, Sina Wittmann, Marcus Jahnel, Raimund Schlüßler, Kyoohyun Kim, Irmela R. E. A. Trussina, Jie Wang, Daniel Mateju, Ina Poser, Shovamayee Maharana, Martine Ruer-Gruß, Doris Richter, Xiaojie Zhang, Young-Tae Chang, Jochen Guck, Alf Honigmann, Julia Mahamid, Anthony A. Hyman, Rohit V. Pappu, Simon Alberti, and Titus M. Franzmann. RNA-Induced Conformational Switching and Clustering of G3BP Drive Stress Granule Assembly by Condensation. *Cell*, 181(2):346–361.e17, April 2020.
- [25] David W. Sanders, Nancy Kedersha, Daniel S. W. Lee, Amy R. Strom, Victoria Drake, Joshua A. Riback, Dan Bracha, Jorine M. Eeftens, Allana Iwanicki, Alicia Wang, Ming-Tzo Wei, Gena Whitney, Shawn M. Lyons, Paul Anderson, William M. Jacobs, Pavel Ivanov, and Clifford P. Brangwynne. Competing Protein-RNA Interaction Networks Control Multiphase Intracellular Organization. *Cell*, 181(2):306–324.e28, April 2020. Publisher: Elsevier.
- [26] Peiguo Yang, Cécile Mathieu, Regina-Maria Kolaitis, Peipei Zhang, James Messing, Ugur Yurtsever, Zemin Yang, Jinjun Wu, Yuxin Li, Qingfei Pan, Jiyang Yu, Erik W. Martin, Tanja Mittag, Hong Joo Kim, and J. Paul Taylor. G3BP1 Is a Tunable Switch that Triggers Phase Separation to Assemble Stress Granules. *Cell*, 181(2):325–345.e28, April 2020. Publisher: Elsevier.

Bibliography

- [27] Marvin E. Tanenbaum, Luke A. Gilbert, Lei S. Qi, Jonathan S. Weissman, and Ronald D. Vale. A Protein-Tagging System for Signal Amplification in Gene Expression and Fluorescence Imaging. *Cell*, 159(3):635–646, October 2014.
- [28] Logan George, Fred E. Indig, Kotb Abdelmohsen, and Myriam Gorospe. Intracellular RNA-tracking methods. *Open Biology*, 8(10), October 2018.
- [29] Christian Genz, Julia Fundakowski, Orit Hermesh, Maria Schmid, and Ralf-Peter Jansen. Association of the Yeast RNA-binding Protein She2p with the Tubular Endoplasmic Reticulum Depends on Membrane Curvature. *The Journal of Biological Chemistry*, 288(45):32384–32393, November 2013.
- [30] Tomas J. Bos, Julia K. Nussbacher, Stefan Aigner, and Gene W. Yeo. Tethered Function Assays as Tools to Elucidate the Molecular Roles of RNA-Binding Proteins. *Advances in experimental medicine and biology*, 907:61–88, 2016.
- [31] Na Yeon Kim, Sangkyu Lee, Jeonghye Yu, Nury Kim, Seong Su Won, Hyerim Park, and Won Do Heo. Optogenetic control of mRNA localization and translation in live cells. *Nature Cell Biology*, 22(3):341–352, March 2020. Number: 3 Publisher: Nature Publishing Group.
- [32] Mauro Ferreira de Azevedo, Paul R. Gilson, Heloisa B. Gabriel, Roseli F. Simões, Fiona Angrisano, Jacob Baum, Brendan S. Crabb, and Gerhard Wunderlich. Systematic Analysis of FKBP Inducible Degradation Domain Tagging Strategies for the Human Malaria Parasite Plasmodium falciparum. *PLOS ONE*, 7(7):e40981, July 2012. Publisher: Public Library of Science.
- [33] Ina Weidenfeld, Manfred Gossen, Rainer Löw, David Kentner, Stefan Berger, Dirk Görlich, Dusan Bartsch, Hermann Bujard, and Kai Schönig.

Bibliography

- Inducible expression of coding and inhibitory RNAs from retargetable genomic loci. *Nucleic Acids Research*, 37(7):e50–e50, April 2009. Publisher: Oxford Academic.
- [34] Jonathan B. Grimm, Brian P. English, Jiji Chen, Joel P. Slaughter, Zhengjian Zhang, Andrey Revyakin, Ronak Patel, John J. Macklin, Davide Normanno, Robert H. Singer, Timothée Lionnet, and Luke D. Lavis. A general method to improve fluorophores for live-cell and single-molecule microscopy. *Nature Methods*, 12(3):244–250, 3 p following 250, March 2015.
 - [35] Jonathan B. Grimm, Anand K. Muthusamy, Yajie Liang, Timothy A. Brown, William C. Lemon, Ronak Patel, Rongwen Lu, John J. Macklin, Philipp J. Keller, Na Ji, and Luke D. Lavis. A general method to fine-tune fluorophores for live-cell and in vivo imaging. *Nature Methods*, 14(10):987–994, October 2017.
 - [36] Johannes H. Wilbertz, Franka Voigt, Ivana Horvathova, Gregory Roth, Yinxiu Zhan, and Jeffrey A. Chao. Single-Molecule Imaging of mRNA Localization and Regulation during the Integrated Stress Response. *Molecular Cell*, 73(5):946–958.e7, 2019.
 - [37] Franka Voigt, Hui Zhang, Xianying A. Cui, Désirée Triebold, Ai Xin Liu, Jan Eglinger, Eliza S. Lee, Jeffrey A. Chao, and Alexander F. Palazzo. Single-Molecule Quantification of Translation-Dependent Association of mRNAs with the Endoplasmic Reticulum. *Cell Reports*, 21(13):3740–3753, December 2017.
 - [38] Caroline Beard, Konrad Hochedlinger, Kathrin Plath, Anton Wutz, and Rudolf Jaenisch. Efficient method to generate single-copy transgenic mice by site-specific integration in embryonic stem cells. *Genesis (New York, N.Y.: 2000)*, 44(1):23–28, January 2006.

Bibliography

- [39] Ivana Horvathova, Franka Voigt, Anna V. Kotrys, Yinxiu Zhan, Caroline G. Artus-Revel, Jan Eglinger, Michael B. Stadler, Luca Giorgetti, and Jeffrey A. Chao. The Dynamics of mRNA Turnover Revealed by Single-Molecule Imaging in Single Cells. *Molecular Cell*, 68(3):615–625.e9, November 2017.
- [40] Johannes Schindelin, Ignacio Arganda-Carreras, Erwin Frise, Verena Kaynig, Mark Longair, Tobias Pietzsch, Stephan Preibisch, Curtis Rueden, Stephan Saalfeld, Benjamin Schmid, Jean-Yves Tinevez, Daniel James White, Volker Hartenstein, Kevin Eliceiri, Pavel Tomancak, and Albert Cardona. Fiji: an open-source platform for biological-image analysis. *Nature Methods*, 9(7):676–682, June 2012.
- [41] Bastian Eichenberger. Fluffy – reproducible deep learning based segmentation of biomedical images., March 2020.
- [42] Michael R. Berthold, Nicolas Cebron, Fabian Dill, Thomas R. Gabriel, Tobias Kötter, Thorsten Meinl, Peter Ohl, Kilian Thiel, and Bernd Wiswedel. KNIME - the Konstanz information miner: version 2.0 and beyond, November 2009.
- [43] Jean-Yves Tinevez, Nick Perry, Johannes Schindelin, Genevieve M. Hoopes, Gregory D. Reynolds, Emmanuel Laplantine, Sebastian Y. Bednarek, Spencer L. Shorte, and Kevin W. Eliceiri. TrackMate: An open and extensible platform for single-particle tracking. *Methods (San Diego, Calif.)*, 115:80–90, 2017.
- [44] Daniel G. Gibson, Lei Young, Ray-Yuan Chuang, J. Craig Venter, Clyde A. Hutchison, and Hamilton O. Smith. Enzymatic assembly of DNA molecules up to several hundred kilobases. *Nature Methods*, 6(5):343–345, May 2009.
- [45] Imre Gaspar, editor. *RNA Detection: Methods and Protocols*. Methods in Molecular Biology. Humana Press, 2018.

Bibliography

- [46] Nobuyuki Otsu. A Threshold Selection Method from Gray-Level Histograms. *IEEE Transactions on Systems, Man, and Cybernetics*, 9(1):62–66, January 1979.
- [47] P. Thévenaz, U. E. Ruttmann, and M. Unser. A pyramid approach to subpixel registration based on intensity. *IEEE transactions on image processing: a publication of the IEEE Signal Processing Society*, 7(1):27–41, 1998.
- [48] Nancy Kedersha, Marc D. Panas, Christopher A. Achorn, Shawn Lyons, Sarah Tisdale, Tyler Hickman, Marshall Thomas, Judy Lieberman, Gerald M. McInerney, Pavel Ivanov, and Paul Anderson. G3BP-Caprin1-USP10 complexes mediate stress granule condensation and associate with 40S subunits. *The Journal of Cell Biology*, 212(7):845–860, March 2016.
- [49] Umber Alam and Derek Kennedy. Rasputin a decade on and more promiscuous than ever? A review of G3BPs. *Biochimica Et Biophysica Acta. Molecular Cell Research*, 1866(3):360–370, 2019.
- [50] Peipei Zhang, Baochang Fan, Peiguo Yang, Jamshid Temirov, James Messing, Hong Joo Kim, and J Paul Taylor. Chronic optogenetic induction of stress granules is cytotoxic and reveals the evolution of ALS-FTD pathology. *eLife*, 8:e39578, March 2019.
- [51] Lihua Chen and Beidong Liu. Relationships between Stress Granules, Oxidative Stress, and Neurodegenerative Diseases. *Oxidative Medicine and Cellular Longevity*, 2017, 2017.
- [52] Jeffrey S. Kieft, Jennifer L. Rabe, and Erich G. Chapman. New hypotheses derived from the structure of a flaviviral Xrn1-resistant RNA: Conservation, folding, and host adaptation. *RNA biology*, 12(11):1169–1177, 2015.

Bibliography

- [53] Sarada Viswanathan, Megan E. Williams, Erik B. Bloss, Timothy J. Stasevich, Colenso M. Speer, Aljoscha Nern, Barret D. Pfeiffer, Bryan M. Hooks, Wei-Ping Li, Brian P. English, Teresa Tian, Gilbert L. Henry, John J. Macklin, Ronak Patel, Charles R. Gerfen, Xiaowei Zhuang, Yalin Wang, Gerald M. Rubin, and Loren L. Looger. High-performance probes for light and electron microscopy. *Nature Methods*, 12(6):568–576, June 2015.
- [54] Ning Zhao, Kouta Kamijo, Philip D. Fox, Haruka Oda, Tatsuya Morisaki, Yuko Sato, Hiroshi Kimura, and Timothy J. Stasevich. A genetically encoded probe for imaging nascent and mature HA-tagged proteins in vivo. *Nature Communications*, 10(1):1–16, July 2019. Number: 1 Publisher: Nature Publishing Group.
- [55] Kimberly M. Bonger, Ling-chun Chen, Corey W. Liu, and Thomas J. Wandless. Small molecule displacement of a cryptic degron causes conditional protein degradation. *Nature chemical biology*, 7(8):531–537, July 2011.
- [56] F. Yang, L. G. Moss, and G. N. Phillips. The molecular structure of green fluorescent protein. *Nature Biotechnology*, 14(10):1246–1251, October 1996.
- [57] Joseph W. Fischer, Veronica F. Busa, Yue Shao, and Anthony K. L. Leung. Structure-Mediated RNA Decay by UPF1 and G3BP1. *Molecular Cell*, 0(0), February 2020. Publisher: Elsevier.
- [58] Hélène Tourrière, Imed-eddine Gallouzi, Karim Chebli, Jean Paul Capony, John Mouaikel, Peter van der Geer, and Jamal Tazi. RasGAP-Associated Endoribonuclease G3BP: Selective RNA Degradation and Phosphorylation-Dependent Localization. *Molecular and Cellular Biology*, 21(22):7747–7760, November 2001.

Bibliography

- [59] Anaïs Aulas, Guillaume Caron, Christos G. Gkogkas, Nguyen-Vi Mohamed, Laurie Destroismaisons, Nahum Sonenberg, Nicole Leclerc, J. Alex Parker, and Christine Vande Velde. G3BP1 promotes stress-induced RNA granule interactions to preserve polyadenylated mRNA. *The Journal of Cell Biology*, 209(1):73–84, April 2015.
- [60] Nadine Bley, Marcell Lederer, Birgit Pfalz, Claudia Reinke, Tommy Fuchs, Markus Glaß, Birgit Möller, and Stefan Hüttelmaier. Stress granules are dispensable for mRNA stabilization during cellular stress. *Nucleic Acids Research*, 43(4):e26, February 2015.
- [61] John D. Laver, Jimmy Ly, Allison K. Winn, Angelo Karaiskakis, Sichun Lin, Kun Nie, Giulia Benic, Nima Jaber-Lashkari, Wen Xi Cao, Alireza Khademi, J. Timothy Westwood, Sachdev S. Sidhu, Quaid Morris, Stephane Angers, Craig A. Smibert, and Howard D. Lipshitz. The RNA-Binding Protein Rasputin/G3BP Enhances the Stability and Translation of Its Target mRNAs. *Cell Reports*, 30(10):3353–3367.e7, March 2020.

A

Supplementary Methods

NLS-stdMCP-stdHalo-G3BP1 cloning primers:

- gattaggatctatcgattactgccgtggcgcaagcccc
- aagttcgtttcagggcccgtatggatggagaagccatgtccct
- ctaggcttccataccatcggccctgaaacagaactt
- gggggcttgcgccacggcagtaatcgatagatctaatacacc

smGCN4-*Renilla*-MS2v5 cloning primers:

- tacacgcggcccaatcatcggtccgggtggatctggaggtggaggttctggaggagaaga
- cctcttccgagccagttccctggcccttattccggttt

Renilla luciferase FISH probes:

- tcgtacacccgttggaaagccat
- agtgatcatgcgttgtcggt
- gttcattgttgcagcgag
- agttgatgaaggaggtccagc
- gcgtgttccgttccgttccgtt
- cagcgttaccatgcagaaaa
- tcgatgtgaggcacgacgt
- gatgtatgttccgttccgtt
- ttaccattccgttccgttccgtt
- gatccaggaggcgatatgag
- caagcggtgagggtacttgc
- ttggaaagggttccgttccgtt

Appendix A. Supplementary Methods

- gtggcccacaaagatgattt
- gagtagtgaaaggccagaca
- ttgatcttgtctggtgctc
- cactctcagcatggacgatg
- caggactcgatcacgtccac
- atatccctcgatgtcagg
- ctcttcgctctgtatcaggg
- attctcaaggcaccatttct
- gcatggtctcgacgaagaag
- tttccgcatgtatctgcttg
- cttaaatggctccaggtagg
- gagagggtaggccgtctaacc
- ttaacgagagggatctcgcg
- gacaatctggacgacgtcgg
- gaaggtaggcgtttagttg
- gaacatcttaggcagatcgt
- tggaaaagaaccagggtcg
- cttagctccctcgacaatag
- ttcacgaactcggtttagg
- cttaaccatttcatctggag
- gctccacgaagctttagt
- tactgctcgttcttcagcac

MS2v4 FISH probes:

- tgccgttttaggttaggatc
- cgcttgaagattggacagtgc
- gactgtaatgacagtggagc
- ctgatgctgctggagttga
- atgtcctgatgttagtcggag
- atcgtcgagcgttgaatgat
- atagtgtctgaggcatgctg
- gtgatgtcgagccgttga

Appendix A. Supplementary Methods

- cgataacgtagaggcagtag
- ctgatgctcgtcgcagaaga
- atctggtatgtccgatgttq

MS2v5 FISH probes:

- tgattgtgaagtgtcgggtg
- tccacccttgttatgtac
- ctgtgtaatgtgtctggagg
- gtgcttctgtttgattggat
- aaatttggtagcagaagccc
- cttgtttagtttttgag
- caggaaatccctgatggta
- ccctcgttgacgtatattg
- gatattcgggaggcgtgatc
- acgcactgaattcgaaagcc
- attcgactctgattggctgc
- ctcttcgcaaagtgcactt
- taagaatggcgcaaggctg
- gtagggagagtgtggttt
- caggaacgctgatgctgttc
- ttcttgagttgggtactg
- tcatgctgcatggggacata
- ttggggatgtattctgggg
- ttggtgctcgatgtgattt
- aagaaaacaacaactccgagcc
- atggagggttgcagtttgc
- ttgtctgttggtagagat
- ctgatgctgcttcgagaaga
- gtatgctcgagtgtttcgaa
- gatcgccacccaagaata
- aattcgtagagatgggtg
- tcgtattggacgtggaacga

Appendix A. Supplementary Methods

- tcgtgatcccgaaaggtaag
 - agtggaaagtgtatgttagctgc
 - atcgtgcattgtcatgttc
 - gttgagacttgtggagcatg
 - tgaacccatggtagtttc
 - tttaggatggaggatgggttc
 - ttgcgcgtttgtggaaaga
 - ttggatgttggaaatgggc
 - gatgcgttaccagtaattgt
 - tagtagtgagagatgtgggc
 - tgctgaacggttggttttt
 - ttgattttccgtgtgttacc
 - gtcttcgtattgttaaacc
 - ttgcgcgtggacgaaagcgtg
 - ccgtccggatgttttgcgtaa
 - cgtttgcgtgttttgcgtga
 - ggttgcgtttgtgggttg
 - ctgagggtttgtatgtacgg

B

Supplementary Figures

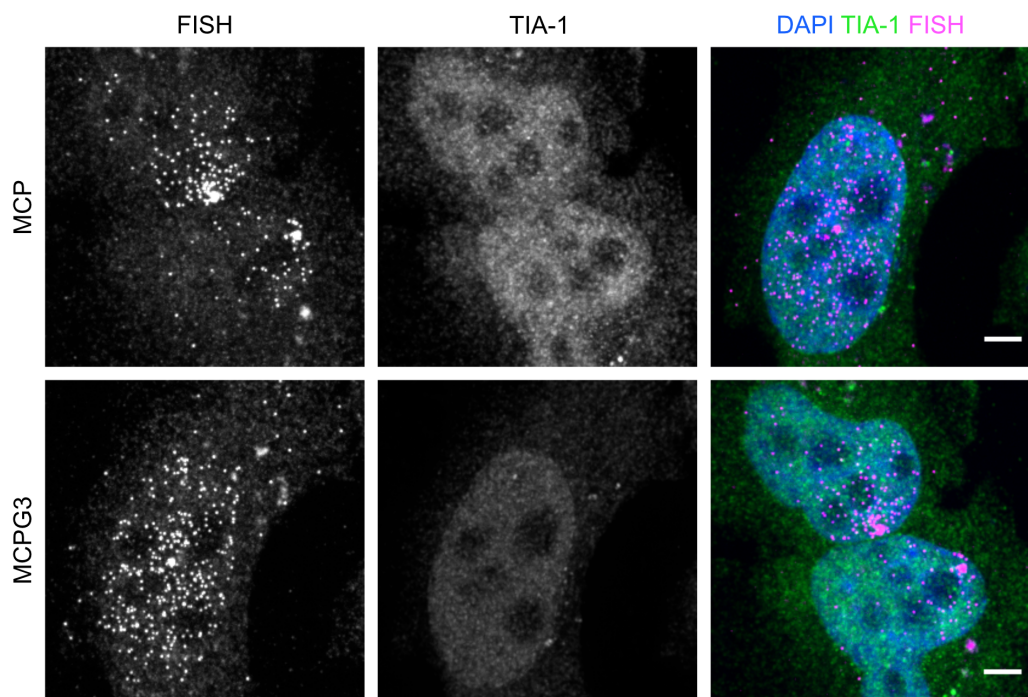


Figure B.1: mRNA localization in non-stressed cells. Representative fluorescence images of the SG marker TIA-1 and the tethered RNAs in unstressed cells. Scale bars, 10 μ m.

Appendix B. Supplementary Figures

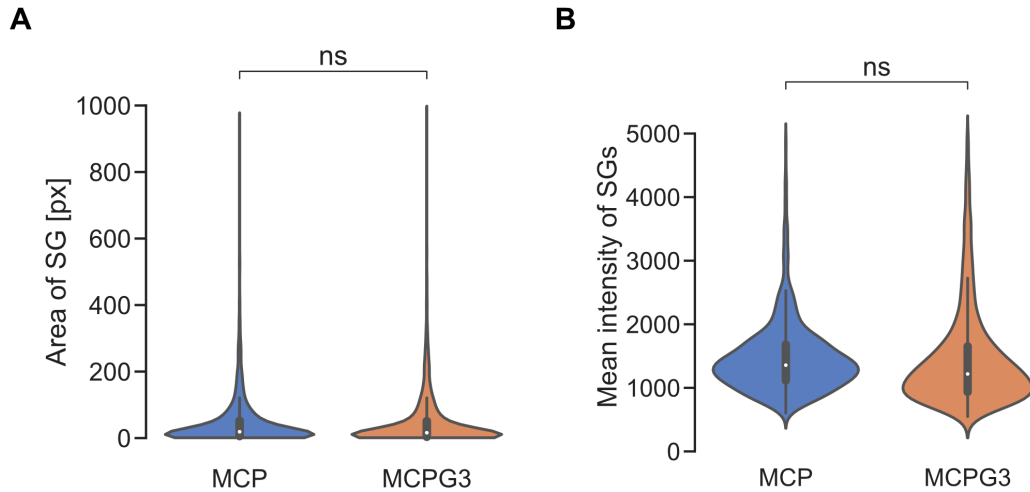


Figure B.2: Comparison of SG properties. (A) SG size comparison between both constructs using a total of 66 cells each. (B) Mean intensity values of single SGs in the TIA-1 SG marker channel.

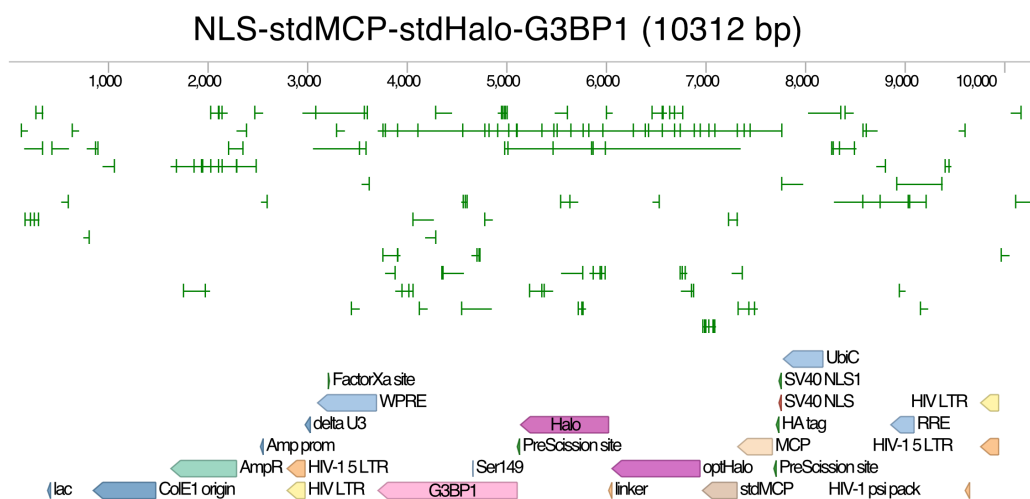


Figure B.3: Design of MCPG3.

Appendix B. Supplementary Figures

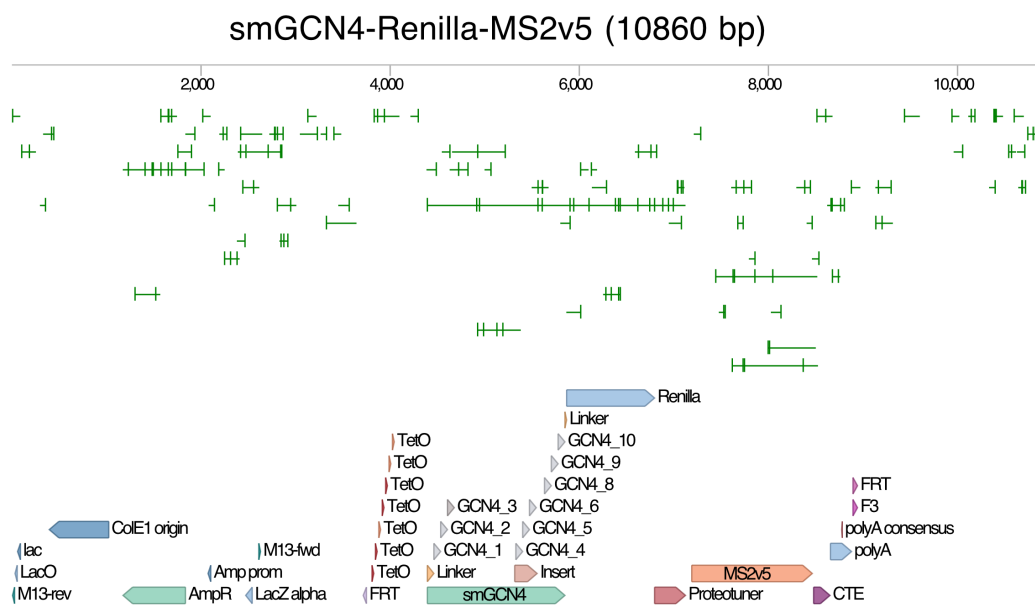


Figure B.4: Design of smGFP SunTag.

Colophon

This document was created using \LaTeX and Bib \TeX typesetting originally developed by Leslie Lamport, based on \TeX created by Donald Knuth.

Theme adapted from a design by Tony Beltramelli.

Edited in Visual Studio Code.

The text is set in Helvetica.